

A NOVEL TIME-DOMAIN PHYSICAL OPTICS FOR COMPUTATION OF ELECTROMAGNETIC SCATTERING OF HOMOGENEOUS DIELECTRIC OBJECTS

Y. Guan, S.-X. Gong, S. Zhang, B. Lu, and T. Hong

National Key Laboratory of Science and Technology on Antennas and Microwaves
Xidian University
Xi'an, Shaanxi 710071, China

Abstract—A novel time-domain physical optics (TDPO) is proposed to determine the transient response of electromagnetic scattering of electrically large homogeneous dielectric targets modeled with triangular facets. Formula of the novel TDPO is derived, in which a time-domain convolution product between the incident plane wave and the time-domain physical-optics (PO) integral is included. The time-domain PO integral is evaluated with a closed-form expression based on a Radon transform interpretation, which makes the novel TDPO highly efficient in speed. The wideband radar cross section (RCS) is conveniently obtained from the transient response with a fast Fourier transform (FFT). Numerical results demonstrate the efficacy of the new method.

1. INTRODUCTION

In recent years, due to the widespread use of short-impulse communication and ultra-wideband radar systems, more and more interests have been focused on the time-domain electromagnetic scattering analysis [1–3]. Time-domain versions of various high-frequency techniques are presented in previous work [4, 5], and the time-domain physical optics (TDPO) plays an important role due to its simplicity and efficiency [6–9]. Ref. [6] extends the concept of the frequency-domain physical-optics (PO) approximation to the time domain and derives the formulas for TDPO (which will be mentioned as the conventional TDPO here and henceforth) to analyze the perfectly

conducting targets. Refs. [7, 8] combine the conventional TDPO with other time-domain methods to calculate the transient scattering of perfectly conducting combinative objects.

So far the TDPO has been widely applied to analysis of perfectly conducting targets. But in the scope of the author's knowledge, it is seldom reported that the homogeneous dielectric object with electrically large size was calculated by the TDPO. Moreover, the time-domain PO integral in the conventional TDPO is evaluated with the tedious and time-consuming numerical integrations, which puts a heavy burden on the computer memory and requires a long solution time. As a result, it is of great importance that the transient scattering of electrically large dielectric objects be determined in an efficient and fast way.

In this paper, a novel version of TDPO is proposed to calculate the transient scattering of electrically large homogeneous dielectric objects. The formula of the novel TDPO is derived with the inverse Fourier transform. This formula contains a time-domain convolution product between the incident plane wave and the time-domain PO integral. The time-domain PO integral is evaluated over the illuminated region of the target with a closed-form expression based on a Radon transform interpretation [10, 11]. Thus the tedious and time-consuming numerical integrations once utilized in the conventional TDPO are avoided, which makes the novel TDPO highly efficient in speed. For illustration purposes, we limit our presentation to the backscattering case. Numerical examples demonstrate the validity and efficiency of the novel TDPO.

2. FORMULAS OF THE NOVEL TDPO

For plane-wave incidence, the frequency-domain scattered electric field of an arbitrary dielectric target predicted by PO can be written as

$$\vec{E}^s(\vec{r}, \omega) = \frac{jk}{4\pi} \frac{e^{-jk r}}{r} \int_{S_l} \left[Z_0 \hat{k}_s \times \hat{k}_s \times \vec{J}_e + \hat{k}_s \times \vec{J}_m \right] e^{jk \hat{k}_s \cdot \vec{r}'} d\vec{r}' \quad (1)$$

where \vec{J}_e and \vec{J}_m are the surface electric current density and magnetic current density on the illuminated surface S_l , respectively, r is the distance of the observation point from the origin, \vec{r}' is the position vector of the surface point corresponding to $d\vec{r}'$, Z_0 is the wave impedance in free space, k is the wave number in free space and \hat{k}_s is the normalized scattered wave vector. \vec{J}_e and \vec{J}_m can be represented

as follows

$$\vec{J}_e = \hat{n}(\vec{r}') \times \vec{H} = \hat{n}(\vec{r}') \times \left[\vec{H}^i(\vec{r}', \omega) + \vec{H}^r(\vec{r}', \omega) \right] \quad (2)$$

$$\vec{J}_m = \vec{E} \times \hat{n}(\vec{r}') = \left[\vec{E}^i(\vec{r}', \omega) + \vec{E}^r(\vec{r}', \omega) \right] \times \hat{n}(\vec{r}') \quad (3)$$

where $\hat{n}(\vec{r}')$ is the unit normal vector at \vec{r}' , $\vec{H}^i(\vec{r}', \omega)$ and $\vec{H}^r(\vec{r}', \omega)$, $\vec{E}^i(\vec{r}', \omega)$ and $\vec{E}^r(\vec{r}', \omega)$ are the incident and reflected magnetic field and electric field at \vec{r}' , respectively.

Substituting (2) and (3) into (1), considering far-field observation and backscattering case, we obtain

$$\vec{E}^s(\vec{r}, \omega) = -\frac{jk}{2\pi} \frac{e^{-jkr}}{r} \int_{S_t} \left[\vec{E}^r(\vec{r}', \omega) (\hat{n}(\vec{r}') \cdot \hat{k}_i) \right] e^{jk\hat{k}_s \cdot \vec{r}'} d\vec{r}' \quad (4)$$

where \hat{k}_i is the normalized incident wave vector, $\hat{k}_i = -\hat{k}_s$.

Using the Fresnel reflection coefficients on the surface of the dielectric target, we express the reflected electric field as [12]

$$\vec{E}^r(\vec{r}', \omega) = \left[R_{\perp}(\vec{r}') E_{\perp}^i(\vec{r}', \omega) \hat{e}_{\perp}(\vec{r}') + R_{//}(\vec{r}') E_{//}^i(\vec{r}', \omega) \hat{e}_{//}(\vec{r}') \right] e^{-jk\hat{k}_i \cdot \vec{r}'} \quad (5)$$

where E_{\perp}^i and $E_{//}^i$ are the E polarization and H polarization components of the frequency-domain incident electric field, respectively, and R_{\perp} and $R_{//}$ are Fresnel reflection coefficients, which can be represented as

$$R_{\perp} = \frac{\eta_2 \cos \theta_i - \eta_1 \cos \theta_t}{\eta_2 \cos \theta_i + \eta_1 \cos \theta_t} \quad (6)$$

$$R_{//} = \frac{\eta_1 \cos \theta_i - \eta_2 \cos \theta_t}{\eta_1 \cos \theta_i + \eta_2 \cos \theta_t} \quad (7)$$

where η_1 and η_2 are the wave impedance for the free space and the dielectric object, respectively, $\eta_i = \sqrt{\frac{\mu_i}{\epsilon_i}}$, $i = 1, 2$. θ_i and θ_t are the incident angle and refracted angle, respectively. Substituting (5) into (4) yields

$$\begin{aligned} \vec{E}^s(\vec{r}, \omega) = & -\frac{jk}{2\pi} \frac{e^{-jkr}}{r} \int_{S_t} \left[R_{\perp}(\vec{r}') E_{\perp}^i(\vec{r}', \omega) \hat{e}_{\perp}(\vec{r}') \right. \\ & \left. - R_{//}(\vec{r}') E_{//}^i(\vec{r}', \omega) \hat{e}_{//}(\vec{r}') \right] \left[\hat{n}(\vec{r}') \cdot \hat{k}_i \right] e^{-j2k\hat{k}_i \cdot \vec{r}'} d\vec{r}' \quad (8) \end{aligned}$$

Assume that the surface S_l is composed of N nonoverlapping triangular facets numbered from 1 to N , (8) can be expressed as

$$\vec{E}^s(\vec{r}, \omega) = -\frac{jk}{2\pi} \frac{e^{-jkr}}{r} \sum_{n=1}^N [R_{\perp n} E_{\perp n}^i(\omega) \hat{e}_{\perp n} - R_{\parallel n} E_{\parallel n}^i(\omega) \hat{e}_{\parallel n}^i] \left(\hat{k}_i \cdot \hat{n}_n \right) h_n(\omega) \quad (9)$$

where

$$h_n(\omega) = \int_{S_n} e^{-2jk\hat{k}_i \cdot \vec{r}'} d\vec{r}' = \int_{S_n} e^{-j\omega(\frac{2}{c})\hat{k}_i \cdot \vec{r}'} d\vec{r}' \quad (10)$$

in which c is the velocity of light in free space. $h_n(\omega)$ can be interpreted as the frequency-domain PO integral. The time-domain representation is obtained with the inverse Fourier transform [10]

$$h_n(t) = \int_{-\infty}^{\infty} h_n(\omega) e^{j\omega t} d\omega = \int_{S_n} \delta\left(t - \frac{2}{c}\hat{k}_i \cdot \vec{r}'\right) d\vec{r}' \quad (11)$$

$h_n(t)$ can be interpreted as the time-domain PO integral.

The novel TDPO formula is obtained by performing the inverse Fourier transform to (9)

$$\vec{E}^s(\vec{r}, t) = -\frac{1}{2\pi cr} \frac{\partial}{\partial t} E^i\left(t - \frac{r}{c}\right) * \sum_{n=1}^N \left[R_{\perp n} (\hat{e}_{\perp n} \cdot \hat{p}) \hat{e}_{\perp n} - R_{\parallel n} (\hat{e}_{\parallel n}^i \cdot \hat{p}) \hat{e}_{\parallel n}^i \right] \left(\hat{k}_i \cdot \hat{n}_n \right) h_n(t) \quad (12)$$

where $E^i(t)$ is the time-domain incident electric field intensity, $\frac{r}{c}$ is the retarded time, \hat{p} is the polarization direction of the incident electric field, and the symbol ‘*’ denotes the convolution product, which is calculated directly in time domain and is defined as

$$f_1(t) * f_2(t) = \sum_{\tau=T_1}^{T_2} f_1(\tau) f_2(t - \tau) \Delta\tau \quad (13)$$

where T_1 and T_2 are the starting time and finish time of the time sequence, respectively, and $\Delta\tau$ is the time step.

It should be noted that when the incident wave vector is perpendicular to the target surface, (12) would be invalid. The transient backscattered field under this condition is calculated by

$$\vec{E}^s(\vec{r}, t) = \frac{A}{2\pi rc} R_{\perp} \frac{\partial}{\partial t} \vec{E}^i\left(t - \frac{r}{c}\right) \quad (14)$$

where A is the area of the target surface.

3. SHADOWING

The time-domain PO integral in (12) is evaluated over the illuminated region of the target surface, so a shadowing processing is performed before the evaluation of the integral. An improved z-buffer algorithm initially used in computer graphics is introduced to perform a fast and accurate shadowing judgment in this paper [13, 14]. Procedure of the shadowing judgment is listed as follows:

- (1) The incident plane wave direction is rotated to $-z$ direction of the Cartesian coordinate system. And the triangular facets that form the whole target are numbered and rotated accordingly. Register z -coordinate of the centroid of each rotated facet.
- (2) The rotated triangular facets are projected to the xoy plane. The projective position of centroid of each facet is calculated and stored. All the facets are initialized to be visible.
- (3) The size of the buffer is determined in terms of the minimum rectangular region that covers the whole projective region. The buffer is then subdivided into many small buffers and each small buffer is numbered. Each small buffer records information of the facets projected into it.
- (4) The shadowing relationship is determined by the depth (z -coordinate of the centroid) comparison of the facets projected into the same buffer or adjacent buffers. A facet is considered to be invisible when it satisfies: 1) It is deeper than another facet in the same small buffer or the surrounding eight small buffers and 2) its centroid locates in the projection of the latter facet.

4. EVALUATION OF THE TIME-DOMAIN PO INTEGRAL

Assume that the area of the n th triangular face S_n is denoted as A_{sn} , and the vertex coordinates of S_n are denoted as \vec{v}_1 , \vec{v}_2 and \vec{v}_3 . By using the Radon transform described in [10], $h_n(t)$ can be written as

$$h_n(t) = \begin{cases} \frac{2A_{sn}}{(t_3 - t_1)(t_2 - t_1)} \frac{(t - t_1)}{(t_2 - t_1)}; & t_1 < t \leq t_2 \\ \frac{2A_{sn}}{(t_3 - t_1)(t_2 - t_3)} \frac{(t - t_3)}{(t_2 - t_3)}; & t_2 < t \leq t_3 \\ 0; & \text{otherwise} \end{cases} \quad (15)$$

where

$$t_i = 2c^{-1} \hat{k}_i \cdot \vec{v}_i, \quad i = 1, 2, 3 \quad (16)$$

The resolved $h_n(t)$ is then substituted into (12) to calculate the transient response of backscattering. Finally the wideband RCS can be obtained with a fast Fourier transform (FFT).

5. NUMERICAL RESULTS

Several examples are given in order to verify the validity and applicability of the novel TDPO.

5.1. Lossless Dielectric Plate

As a first example, we consider the impulsive plane-wave backscattering from a dielectric rectangular plate shown in Fig. 1. The plate is lying on the x - z plane with a size of $0.6\text{ m} \times 0.5\text{ m}$. The dielectric plate has a relative dielectric permittivity $\varepsilon_r = 4.0$ and a relative magnetic permeability $\mu_r = 1.0$. A modulated Gaussian-impulse plane wave with a bandwidth from 10 GHz to 40 GHz and a center frequency of 25 GHz illuminates the plate normally. The time-domain incident electric field is expressed as

$$\vec{E}^i(t) = \hat{z} \cos(1.57 \times 10^{11}t) \cdot \exp\left[-\frac{4\pi(t - 1.07 \times 10^{-10})^2}{(1.33 \times 10^{-10})^2}\right] \quad (17)$$

The transient response of the backscattering of the plate is computed by the novel TDPO. It is noted that the convolution product in (12) is calculated directly in time domain. Usually, it is common for the calculation of a convolution product in time domain to resort to the product directly in the frequency domain and then come back in time domain with an inverse fast Fourier transform (IFFT). As a consequence, a similar calculation procedure, named Gordon-IFFT method, is implemented as a reference by using the Gordon formula [15] to compute the frequency-domain response and then applying an IFFT to obtain the time-domain response. The $\theta\theta$ polarized transient response results obtained by different methods are plotted in Fig. 1. The transient response of a perfectly conducting plate with the same size is also calculated and shown in Fig. 1 as a reference. The transient response of the perfectly conducting plate is obtained by the conventional TDPO and Gordon-IFFT method. It can be seen that the two results of the dielectric plate are well compatible, which illustrates the validity of the novel TDPO. It is found that the magnitude of the scattered field of the dielectric plate is smaller than that of the perfectly conducting plate. The reason is that total reflection happens on the perfectly conducting surface while only part of the incident energy is reflected on the dielectric surface. For a further verification,

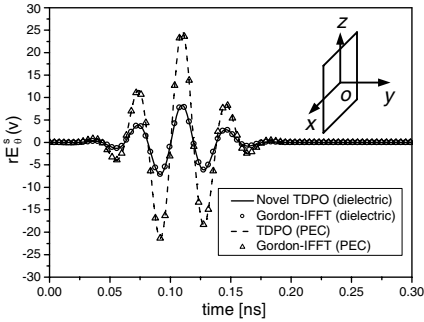


Figure 1. Transient response of backscattering from the rectangular plate. (Inset: The model of the rectangular plate).

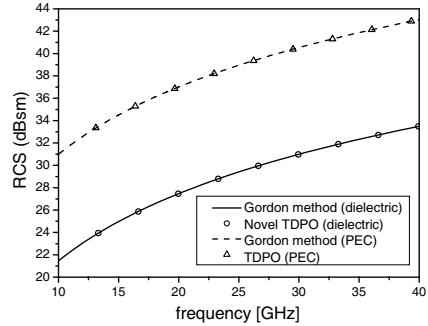


Figure 2. Wideband monostatic RCS of the rectangular plate.

the wideband monostatic RCS is calculated with a FFT and compared with that obtained by a frequency sweep procedure based on Gordon formula. The wideband RCS results are shown in Fig. 2. The good agreement of the two results of the dielectric plate again demonstrates the validity of the novel TDPO. The RCS of the dielectric plate is smaller than that of the perfectly conducting plate for the reason mentioned above.

5.2. Lossless Dielectric Sphere-cone

As a second example, the backscattering from a sphere-cone for Gaussian-impulse plane-wave incidence is considered. The sphere-cone, which is a simplified model of a missile, is shown in Fig. 3. The sphere-cone is composed of a spherical cap and a cone. The half cone angle is $\alpha = 7^\circ$, the radius of the spherical cap is 0.0749 m, and the lengths of the cone and the whole sphere-cone are 0.6051 m and 0.6891 m, respectively. The sphere cone has a relative dielectric permittivity $\epsilon_r = 4.0$ and a relative magnetic permeability $\mu_r = 1.0$. A Gaussian-impulse plane wave with a bandwidth from 0 to 10 GHz illuminates the model along the $-\hat{x}$ direction. The time-domain incident electric field is written as

$$\vec{E}^i(t) = \hat{y} \exp \left[-\frac{4\pi (t - 1.6 \times 10^{-10})^2}{(2 \times 10^{-10})^2} \right] \quad (18)$$

In order to ensure that the target is electrically large in dimension, the effective bandwidth from 5 GHz to 10 GHz is concerned in the

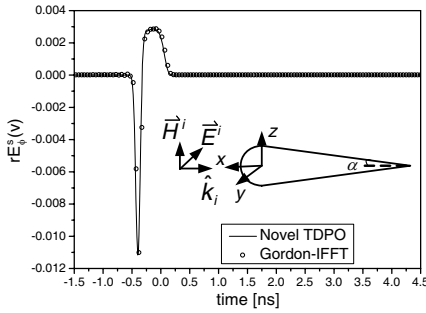


Figure 3. Transient response of backscattering from a dielectric sphere-cone. (Inset: The model of the sphere-cone).

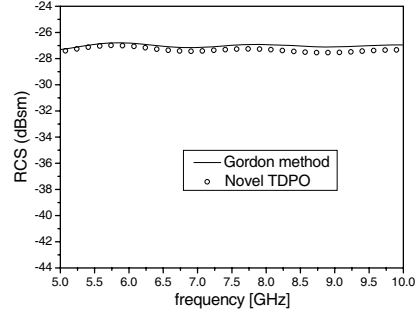


Figure 4. Wideband monostatic RCS of the dielectric sphere-cone.

following analysis. The $\phi\phi$ polarized transient response results obtained by different methods are shown in Fig. 3. It can be seen that the two results are in good agreement. The wideband monostatic RCS results are given in Fig. 4, which are also well compatible. Thus the validity of the novel TDPO is demonstrated through all these comparisons.

5.3. Lossy Dielectric Plate

The targets considered in the above two examples are lossless. Hence, the backscattering from a lossy dielectric plate is calculated in this section. The dielectric plate is made from carbon fiber and has a relative dielectric permittivity $\epsilon_r = 439.81 - j227.19$ and a relative magnetic permeability $\mu_r = 1.0$. The size of the plate and the incident Gaussian impulse are the same as those described in Sec. 5.1. The $\theta\theta$ polarized transient response results obtained by novel TDPO and Gordon-IFFT method are plotted in Fig. 5. It can be seen that the results are in a good agreement. The wideband monostatic RCS results are shown in Fig. 6, which are also well compatible.

5.4. Combined Model

In order to further demonstrate the validity of the shadowing technique provided in Sec. 3, the backscattering from a combined model is discussed in this section. Fig. 7 shows a dielectric sphere of radius 0.2 m placed above a dielectric plate with a size of 0.6 m \times 0.6 m. The distance between the center of the sphere and the plate is 0.3 m. Both

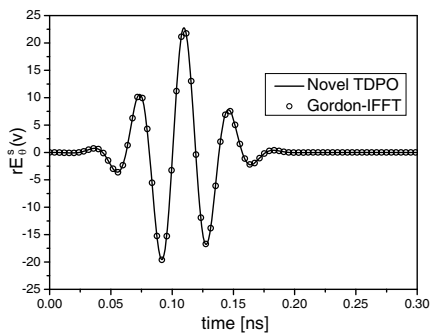


Figure 5. Transient response of backscattering from a lossy dielectric plate.

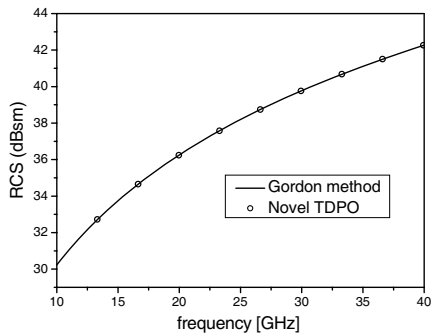


Figure 6. Wideband monostatic RCS of the lossy dielectric plate.

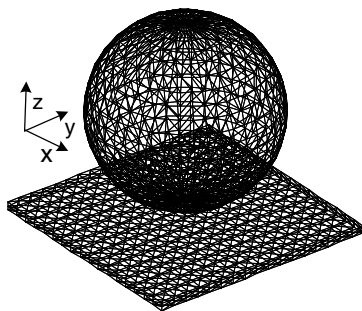


Figure 7. Triangular facets subdivision of the combined model.

the sphere and the plate have a relative dielectric permittivity $\epsilon_r = 4.0$ and a relative magnetic permeability $\mu_r = 1.0$. A modulated Gaussian-impulse plane wave with a bandwidth from 10 GHz to 20 GHz and a center frequency of 15 GHz illuminates the combined model along $-z$ direction. The time-domain incident electric field can be expressed as

$$\vec{E}^i(t) = -\hat{x} \cos(9.42 \times 10^{10}t) \exp\left[-\frac{4\pi(t - 3.2 \times 10^{-10})^2}{(4 \times 10^{-10})^2}\right] \quad (19)$$

The $\theta\theta$ polarized transient response results obtained by different methods are given in Fig. 8. Multiple scattering is not taken into account here for simplicity. It can be seen from Fig. 8 that the two results show good agreement. The wideband monostatic RCS results are shown in Fig. 9, which are also well compatible. Thus the shadowing technique is proved to be valid.

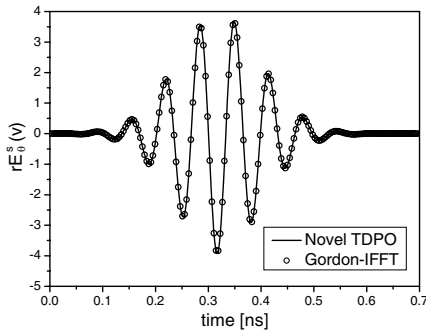


Figure 8. Transient response of backscattering from the dielectric combined model.

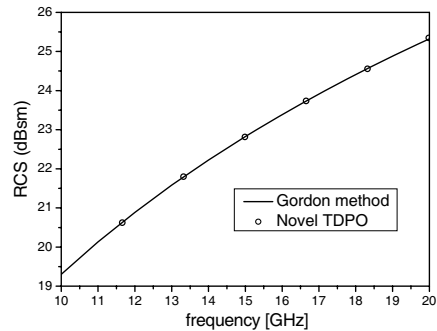


Figure 9. Wideband monostatic RCS of the dielectric combined model.

Table 1. Comparison of solution time between different methods (unit: second).

Number of triangular facets	Solution time of Gordon-IFFT	Solution time of novel TDPO
640	14.2	0.2
2462	189.8	1.0
9748	2966.8	9.8

5.5. Speed Analysis

The speed superiority of the novel TDPO over the Gordon-IFFT method is examined as follows. The novel TDPO is a time-domain technique, and the time-domain PO integral is evaluated with a closed-form expression based on Radon transform, which avoids the utilization of numerical integrations. As a result, the novel TDPO is faster than the Gordon-IFFT method, in which a frequency sweep procedure is required. A comparison of solution time of different methods is given below for the model shown in Fig. 3. Assume that the wavelength corresponding to the highest frequency of the Gaussian impulse is denoted as λ_c . When the high threshold of the edge length of each triangular facet is set as $\lambda_c/4$, $\lambda_c/2$ and λ_c , the number of facets that form the sphere-cone will be 9748, 2462 and 640, respectively. With the codes running on a PC with a 3.0 GHz Core 2 Duo processor, the solution time of the novel TDPO and Gordon-IFFT method is compared in Table 1.

It can be found that the solution time of the novel TDPO is much less than that of the Gordon-IFFT method. Moreover, the more triangular facets there are, the more obvious the time superiority of the novel TDPO is, which is of great value to the transient response analysis of electrically large targets.

6. CONCLUSION

A novel TDPO is proposed to compute the transient response of scattering of homogeneous dielectric targets modeled by triangular facets. Formula for the novel TDPO is derived with an inverse Fourier transform. The time-domain PO integral in the formula is evaluated by a closed-form expression based on a Radon transform interpretation. The transient response is obtained through a direct time-domain convolution product between the incident electric field and the time-domain PO integral. Numerical examples demonstrate the validity and speed superiority of the novel TDPO. Time-domain multiple scattering is not taken into account in this paper, which is the author's attention now and will be reported in the future.

REFERENCES

1. Shanker, B., M. Lu, J. Yuan, and E. Michielssen, "Time domain integral equation analysis of scattering from composite bodies via exact evaluation of radiation fields," *IEEE Trans. Antennas Propag.*, Vol. 57, No. 5, 1506–1520, May 2009.
2. Meng, R., Z. Dongming, L. Ying, and H. Jianguo, "Coupled TDIE-PO method for transient scattering from electrically large conducting objects," *Electron. Lett.*, Vol. 44, No. 4, 258–259, Feb. 2008.
3. Zhang, G. H. and M. Y. Xia, "Time domain integral equation approach for analysis of transient response by metallic-dielectric composite bodies," *Progress In Electromagnetics Research*, Vol. 87, 1–14, 2008.
4. Veruttipong, T. W., "Time domain version of the uniform GTD," *IEEE Trans. Antennas Propag.*, Vol. 38, No. 11, 1757–1764, Nov. 1990.
5. Johansen, P. M., "Time-domain version of the physical theory of diffraction," *IEEE Trans. Antennas Propag.*, Vol. 47, No. 2, 261–270, Feb. 1999.
6. Sun, E.-Y. and W. V. T. Rusch, "Time-domain physical-optics," *IEEE Trans. Antennas Propag.*, Vol. 42, No. 1, 9–15, Jan. 1994.

7. Yang, L.-X., D.-B. Ge, and B. Wei, "FDTD/TDPO hybrid approach for analysis of the EM scattering of combinative objects," *Progress In Electromagnetics Research*, Vol. 76, 275–284, 2007.
8. Faghihi, F. and H. Heydari, "A combination of time domain finite element-boundary integral with time domain physical optics for calculation of electromagnetic scattering of 3-D structures," *Progress In Electromagnetics Research*, Vol. 79, 463–474, 2008.
9. Faghihi, F. and H. Heydari, "Time domain physical optics for the higher-order FDTD modeling in electromagnetic scattering from 3-D complex and combined multiple materials objects," *Progress In Electromagnetics Research*, Vol. 95, 87–102, 2009.
10. Bölükbas, D. and A. A. Ergin, "A Radon transform interpretation of the physical optics integral," *Microw. Opt. Technol. Lett.*, Vol. 44, No. 3, 284–288, Feb. 2005.
11. Serim, H. A. and A. A. Ergin, "Computation of the physical optics integral on NURBS surfaces using a Radon transform interpretation," *IEEE Antennas Wireless Propag. Lett.*, Vol. 7, 70–73, 2008.
12. Klement, D., J. Preissner, and V. Stein, "Special problems in applying the physical optics method for backscatter computation of combined objects," *IEEE Trans. Antennas Propag.*, Vol. 36, No. 2, 228–237, Feb. 1988.
13. Rius, J. M., M. Ferrando, and L. Jofre, "High-frequency RCS of complex radar targets in real-time," *IEEE Trans. Antennas Propag.*, Vol. 41, No. 9, 1308–1319, Sep. 1993.
14. Zha, F.-T., S.-X. Gong, Y.-X. Xu, Y. Guan, and W. Jiang, "Fast shadowing technique for electrically large targets using z-buffer," *Journal of Electromagnetic Waves and Applications*, Vol. 23, Nos. 2–3, 341–349, 2009.
15. Gordon, W. B., "Far-field approximation to the Kirchhoff-Helmholtz representations of scattered fields," *IEEE Trans. Antennas Propag.*, Vol. 23, No. 7, 590–592, Jul. 1975.